J|A|C|S
ARTICLES
Published on Web 12/22/2001

From Local Adsorption Stresses to Chiral Surfaces: (*R*,*R*)-Tartaric Acid on Ni(110)

Vincent Humblot,[†] Sam Haq,[†] Chris Muryn,[†] Werner A. Hofer,[‡] and Rasmita Raval*[,†]

Contribution from the Leverhulme Centre for Innovative Catalysis and Surface Science Research Centre, Department of Chemistry, University of Liverpool, Liverpool L69 7ZD, United Kingdom, and Department of Physics and Astronomy, University College London, Gower Street, London WC1E 6BT, United Kingdom

Received August 21, 2001

Abstract: The chiral molecule (*R*,*R*)-tartaric acid adsorbed on nickel surfaces creates highly enantioselective heterogeneous catalysts, but the nature of chiral modification remains unknown. Here, we report on the behavior of this chiral molecule with a defined Ni(110) surface. A combination of reflection absorption infrared spectroscopy, scanning tunneling microscopy, and periodic density functional theory calculations reveals a new mode of chiral induction. At room temperatures and low coverages, (*R*,*R*)-tartaric acid is adsorbed in its bitartrate form with two-point bonding to the surface via both carboxylate groups. The molecule is preferentially located above the 4-fold hollow site with each carboxylate functionality adsorbed at the short bridge site via O atoms placed above adjacent Ni atoms. However, repulsive interactions between the chiral OH groups of the molecule and the metal atoms lead to severely strained adsorption on the bulk-truncation Ni(110) surface. As a result, the most stable adsorption structure is one in which this adsorption-induced stress is alleviated by significant relaxation of surface metal atoms so that a long distance of 7.47 Å between pairs of Ni atoms can be accommodated at the surface. Interestingly, this leads the bonding Ni atoms to describe a *chiral* footprint at the surface for which all local mirror symmetry planes are destroyed. Calculations show only one chiral footprint to be favored by the (*R*,*R*)-tartaric acid, with the mirror adsorption site being unstable by 6 kJ mol^{-1}. This energy difference is sufficient to enable the same local chiral reconstruction and motif to be sustained over 90% of the system, leading to an overall highly chiral metal surface.

1. Introduction

The emphasis in surface science research is increasingly focused toward the understanding of surface functionality on the nanoscale. In particular, the functionalized organic/inorganic interface has attracted growing attention due to its versatility and wide range of technical applications. Recently, attempts have been made to bestow the ultimate functionality of organic molecules, that is, chirality, onto naturally achiral metal surfaces.[1−7] The application of such chiral surfaces ranges from heterogeneous enantioselective catalysis to chemical sensors, chiral separations, and nonlinear optical devices. In heterogeneous catalysis, chirality has been successfully bestowed onto metal surfaces by the adsorption of chiral organic molecules, leading to highly stereoselective catalysts.[8−15] Currently, the most successful heterogeneous catalytic reaction is the hydrogenation of β-ketoesters over supported nickel catalysts.[8−15] Here, enantioselectivity is induced by the adsorption of chiral modifier molecules on the Ni surface, with (*R*,*R*)-tartaric acid providing one of the best performances, controlling hydrogenation of the simplest β-ketoester, methylacetoacetate, to an enantiomeric excess (e.e.) of over 90% for the *R* enantiomer.[8,9] The main drive of our research has been to create a fundamental understanding on the nanoscale of such systems. Recently, we have shown that (*R*,*R*)-tartaric acid produces an extended chiral surface on Cu(110), assembling in highly organized structures which possess growth directions that destroy all the mirror symmetry planes of the underlying metal surface.[1,2,4,5] It is emphasized that the "handedness" created by this adsorption

* To whom correspondence should be addressed. E-mail: Raval@liv.ac.uk. Tel: +44 151 794 3584. Fax: +44 151 794 3265.
[†] University of Liverpool.
[‡] University College London.

(1) Ortega-Lorenzo, M.; Baddeley, C. J.; Muryn, C.; Raval, R. *Nature* **2000**, *404*, 376.
(2) Ortega-Lorenzo, M.; Haq, S.; Bertrams, T.; Murray, P.; Raval, R.; Baddeley, C. J. *J. Phys. Chem.* **1999**, *103*, 10661.
(3) Williams, J.; Haq, S.; Raval, R. *Surf. Sci.* **1996**, *368*, 303.
(4) Raval, R.; Baddeley, C. J.; Haq, S.; Louafi, S.; Murray, P.; Muryn, C.; Ortega-Lorenzo, M.; Williams, J. *Stud. Surf. Sci. Catal.* **1999**, *122*, 11.
(5) Raval, R. CATTECH **2001**, *5*, 12.
(6) Ernst, K.-H.; Neuber, M.; Grunze, M.; Ellerbeck, U. *J. Am. Chem. Soc.* **2001**, *123*, 493.
(7) De Feyter, S.; Gesquière, A.; Abdel-Mottaleb, M. M.; Grim, P. C. M.; De Shryver, F. C.; Meiners, C.; Sieffert, M.; Valiyaveettil, S.; Müllen, K. *Acc. Chem. Res.* **2000**, *33*, 520.
(8) Izumi, Y. *Adv. Catal.* **1983**, *32*, 215.
(9) Tai, A.; Harada, T. In *Tailored Metal Catalysts*; Iwasawa, Y., Ed.; D. Reidel Publishing Company: Dordrecht, The Netherlands, 1986; p 265.
(10) Tai, A.; Harada, T.; Hiraki, Y.; Murakami, S. *Bull. Chem. Soc. Jpn.* **1983**, *56*, 1414.
(11) Baiker, A.; Blaser, H. U. In *Handbook of Heterogeneous Catalysis*; Ertl, G. H., Knoezinger, H., Weinheim, J., Eds.; VCH: New York, 1997; Vol. 5, p 2422.
(12) Blaser, H. U. *Tetrahedron: Asymmetry* **1991**, *2*, 843.
(13) Baiker, A. *Curr. Opin. Solid State Mater. Sci.* **1998**, *3*, 86.
(14) Webb, G.; Wells, P. B. *Catal. Today* **1992**, *12*, 319.
(15) Keane, M. A.; Webb, G. *J. Catal.* **1992**, *136*, 1.

structure is sustained over the entire surface which is, therefore, truly chiral. This is fundamentally different from the reports of local chirality induced by organic molecules at metal surfaces,[16−18] but where both mirror twins are equally allowed, leading to an overall racemic system.

In this paper, we turn from the Cu surface to the Ni surface, which is the metal most commonly used in the successful catalytic system, and report on the nature of chiral modification of Ni(110) by (*R*,*R*)-tartaric acid. We have utilized a multidisciplinary approach to identify the adsorption of (*R*,*R*)-tartaric acid on the nickel surface. For the local ordering on the nanoscale, we used a scanning tunneling microscope (STM), while the long-range ordering of the adsorbed molecules was established by low-energy electron diffraction (LEED). The chemical nature and orientation of the adsorbed species were analyzed by reflection absorption infrared spectroscopy (RAIRS). Finally, to gain a deeper understanding of the adsorption energetics, we performed extensive ab initio calculations within the density functional theory (DFT) approach to ground-state properties.

2. Experimental Methods

Experiments were conducted in two separate ultrahigh vacuum (UHV) chambers. The first chamber, mainly dedicated to RAIRS, contained facilities for temperature-programmed desorption (TPD), LEED, Auger electron spectroscopy (AES), and sample cleaning. This chamber was interfaced with a commercial Mattson 6020 FTIR spectrometer equipped with a liquid nitrogen cooled HgCdTe detector possessing a spectral range of 650−4000 cm^{-1}. RAIR spectra were collected throughout a continuous dosing regime as sample single beam infrared spectra and ratioed against a background single beam reference of the clean nickel surface. All spectra were obtained at 4 cm^{-1} resolution with coaddition of 200 scans. STM experiments were conducted in a second Omicron Vakuumphysik chamber with facilities for STM, LEED, AES, and sample cleaning. STM experiments were carried out with the sample at room temperature, and the images were acquired in constant current mode.

The nickel crystals were provided by Surface Preparation Laboratory (Netherlands) with a purity of 99.99% (4 N) and alignment accuracies of 0.5° and 0.1° for the RAIRS and the STM experiments, respectively. In each chamber, the Ni(110) crystal was cleaned by cycles of Ar^+ ion sputtering, flashing, and annealing at 900 K. The surface cleanliness and ordering were monitored by AES and LEED. (*R*,*R*)-tartaric acid (99%) was obtained from Sigma-Aldrich Chemicals and was used without any further purification. The sample was contained in a small resistively heated glass tube, separated from the main chamber by a gate valve, and differentially pumped by a turbo molecular pumping system. Before sublimation, tartaric acid was outgassed at 330 K and was then heated to 370 K and exposed to the nickel crystal. During sublimation, the main chamber base pressure was typically 2×10^{-9} mbar.

3. Theoretical Methods

It is customary in solid-state physics to carry out calculations of this kind with periodic systems, rather than with cluster models. Our calculations were performed with the Vienna ab initio simulation package (VASP).[19,20] This code is based on periodic supercells, where one supercell comprises the bulk and surface of a crystal as well as the attached molecules and the vacuum above this surface. The program utilizes pseudopotentials for the ions and the core electrons;[21,22] the ground state of the valence electrons is determined by an energy minimization scheme equivalent to a system of one-particle Schrödinger equations. From this ground state, the Hellmann-Feynman forces on the ions are determined. Ground-state adsorption sites and their energies then follow from an efficient minimization scheme for the forces on all ions.[23,24] The calculations were done for a (3×3) Ni(110) surface, with four Ni layers separated by a vacuum layer of 12 Å. The system size, which is at the current limit of what is tractable within a reasonable time scale, was necessary for a full relaxation of the surface atoms in various initial configurations of the adsorbed (*R*,*R*)-tartaric acid molecule. On the technical side we note that due to the large unit cell, the k-point sampling could be reduced to $(3 \times 2 \times 1)$ special points of a Monkhorst-Pack grid.[25] The forces on the ions in the final consistency loops were less than 0.01 eV/Å. All relaxations were done in a paramagnetic calculation, since it was shown recently that the ground-state positions of Ni atoms do not vary by more than a few hundredths of one angstrom if spin-up and spin-down states are computed separately.[26] The interlayer spacing between the first three layers in the initial configuration of the Ni surface was also taken from the same first principles calculations.[26] In our simulation of molecular adsorption, we only relaxed the surface Ni layer, while the second layer was kept rigid. From the small relaxations of surface atoms (less than 0.1 Å), we conclude that this does not impose unrealistic limitations on the system. The adsorption energies were checked by performing spin-polarized calculations. The absolute differences we found between the two methods are less than 0.1 eV. However, the relative differences between different adsorption sites are much lower and below the range of surface energies. We also checked the convergence of our results by performing additional spin-polarized energy calculations at the relaxed positions with a grid of $(6 \times 4 \times 1)$ k-points.

4. Results and Discussion

Figure 1 shows the STM data obtained with increasing coverage of (*R*,*R*)-tartaric acid on Ni(110) at room temperature. From these, it can be seen that no long-range ordered structures of the type observed on Cu(110)[1,2] are formed. Initial adsorption, Figure 1a, leads to random occupation of surface sites, with a statistical distribution of single, double, triplet, etc. aggregations. However, despite the lack of two-dimensional ordering, Figure 1 shows that all the adsorbed molecules exhibit a very preferred growth direction along the main $<1\bar{1}0>$ direction. This is more clearly observed at higher coverages, Figure 1c, when the adsorbed molecules organize into chains oriented along the close-packed crystallographic axis, which also coincides with a mirror symmetry direction of the surface. Again, this behavior is very different from that observed for Cu(110), where the

(16) Schunack, M.; Laegsgaard, E.; Stensgaard, I.; Johannsen, I.; Besenbacher, F. *Angew. Chem., Int. Ed.* **2001**, *40*, 2623.
(17) Lopinski, G. P.; Moffat, D. J.; Wayner, D. D. M.; Wolkov, R. A. *Nature* **1998**, *39*, 909.
(18) Viswanathn, R.; Zasadzinski, J. A.; Schwartz, D. K. *Nature* **1994**, *368*, 440.
(19) Kresse, G.; Hafner, J. *Phys. Rev. B: Condens. Matter* **1993**, *47*, R558.
(20) Kresse, G.; Furthmueller, J. *Phys. Rev. B: Condens. Matter* **1996**, *54*, 11169.
(21) Vanderbilt, D. *Phys. Rev. B: Condens. Matter* **1990**, *41*, 7892.
(22) Perdew, J. P.; Chevary, J. A.; Vosko, S. H.; Jackson, K. A.; Pederson, M. R.; Singh, D. J.; Fiolhais, C. J. *Phys. Rev. B: Condens. Matter* **1992**, *46*, 6671.
(23) Car, R.; Parinello, M. *Phys. Rev. Lett.* **1985**, *55*, 2471.
(24) Payne, M. C.; Teter, M. P.; Allan, D. C.; Arias, T. A.; Joannopoulos, J. D. *Rev. Mod. Phys.* **1992**, *64*, 1045.
(25) Monkhorst, H. J.; Pack, J. D. *Phys. Rev. B: Condens. Matter* **1976**, *13*, 5188.
(26) Mittendorfer, F.; Eichler, A.; Hafner, J. *Surf. Sci.* **1999**, *423*, 1.

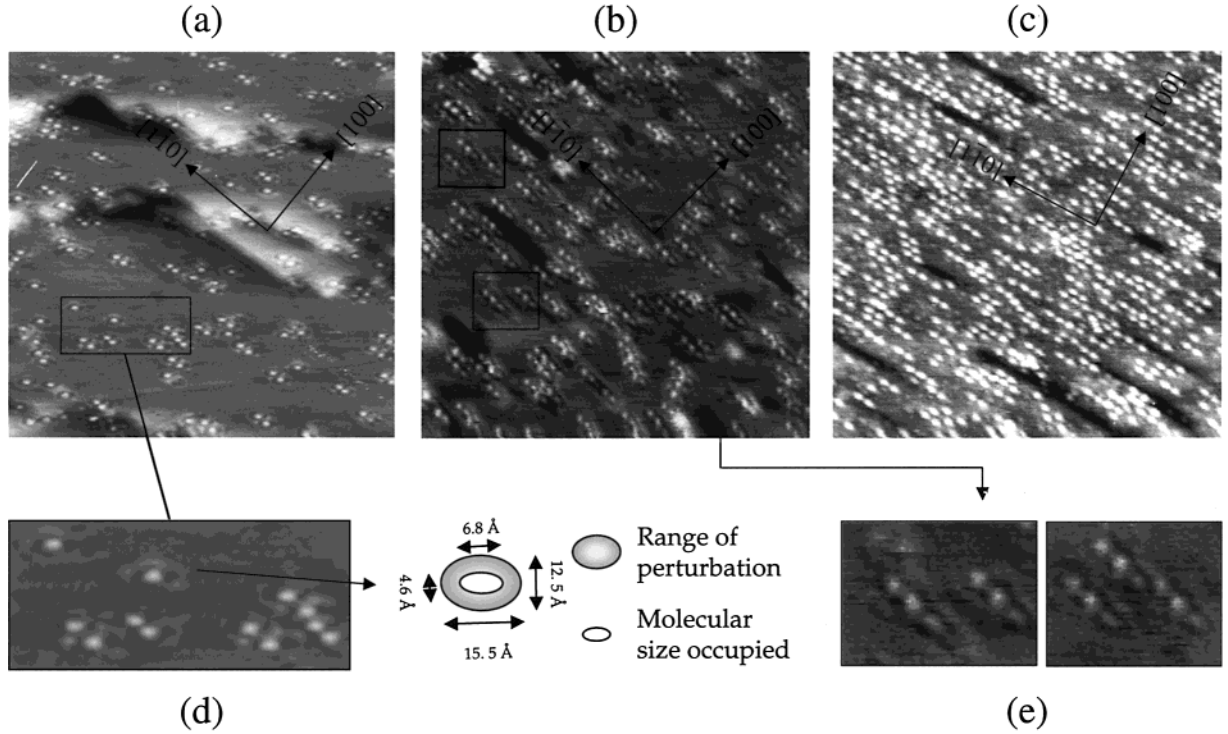

Figure 1. STM images obtained with increasing coverage from (a) to (c) of (*R*,*R*)-tartaric acid on Ni(110) at room temperature. (a) 300 × 300 Å^2 image with $V_{tip} = -2.115$ V and $I_t = 1.16$ nA; (b) 300 × 300 Å^2 image with $V_{tip} = -1.467$ V and $I_t = 1$ nA; (c) 300 × 300 Å^2 image with $V_{tip} = -1.76$ V and $I_t = 1$ nA. In (a), areas of flat terraces are shown alongside step edges. In (b) and (c), the areas imaged as long dark stripes are due to coadsorbed H atoms, which are produced during the chemisorption process via a double deprotonation of the (*R*,*R*)-tartaric acid molecule. The H atoms segregate in separate islands and are thought to be adsorbed in a local missing-row structure.[27,28] Finally, the detail of the local distortion caused by adsorption is shown in (d), which shows a 45 × 100 Å^2 zoom of (a) with molecular size and range of perturbation identified, and in (e), which shows a 45 × 50 Å^2 zoom of the outlined areas in (b).

molecules assemble along nonsymmetry directions,[1,2] thus annihilating all the mirror planes. In view of this, one is faced with the following question: How is chirality communicated to the nickel surface? To answer this, a fundamental understanding of the local adsorption structures created by (*R*,*R*)-tartaric acid is required. This detail is not generally accessible from STM images, so one has to turn to other surface molecular spectroscopies and theoretical modeling to elicit this information. For the present study, we have utilized surface infrared spectroscopy and density functional theory.

4.1. Local Chemical Nature of the (*R*,*R*)-Tartaric Acid Molecule. (*R*,*R*)-tartaric acid, or L-(+)-2,3-dihydroxysuccinic acid, is a chemically adaptable molecule, which can exist in at least three different forms: the neutral biacid form, the monotartrate form where one of the carboxylic acid groups is deprotonated, and the bitartarte form, where both acid groups are deprotonated producing two carboxylate functionalities. The vibrational band structure for each form is different,[29−31] so they may be distinguished by IR spectroscopy. For example, the presence of the carboxylate group is signaled by the appearance of the ν_{OCO}^{asym} and the ν_{OCO}^{sym} vibrations around 1600 and 1400 cm^{-1}, respectively, while the carboxylic acid group is indicated by distinct $\nu_{C=O}$ and ν_{C-O} vibrations around 1750 and 1380 cm^{-1}, respectively.[32] The use of reflection absorption infrared spectroscopy (RAIRS) with a metal surface also allows the orientation of the different functional groups of the adsorbate to be deduced by the application of dipole selection rules,[33,34] which specify that only vibrational modes with a dipole moment change perpendicular to the surface will be observed.

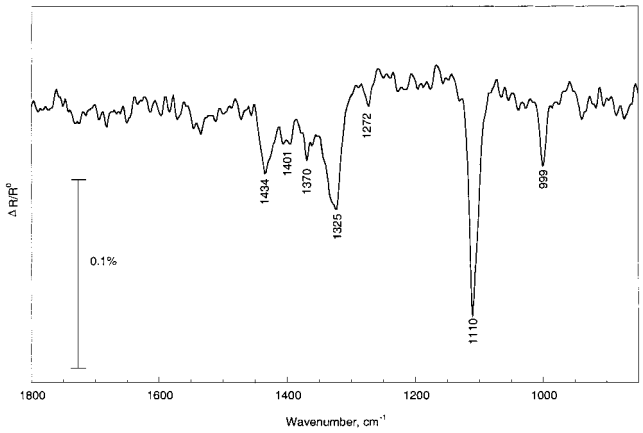

Figure 2. RAIR spectrum obtained at a low coverage of (*R*,*R*)-tartaric acid on Ni(110) at 300 K.

The RAIR spectrum for low coverages of (*R*,*R*)-tartaric acid adsorbed on Ni(110) at 300 K is shown in Figure 2. A

(27) Nielsen, L. P.; Besenbacher, F.; Laegsgaard, E.; Stensgaard, I. *Phys. Rev. B: Condens. Matter* **1991**, *44*, 13156.
(28) Sprunger, P. T.; Okawa, Y.; Besenbacher, F.; Stensgaard, I.; Tanaka, K. *Surf. Sci*. **1995**, *344*, 98.
(29) Bhattacharjee, R.; Jain, Y. S.; Bist, H. D. *J. Raman Spectrosc.* **1989**, *20*, 91.
(30) Bhattacharjee, R.; Jain, Y. S.; Raghubanshi, G.; Bist, H. D. *J. Raman Spectrosc.* **1988**, *19*, 51.
(31) Srivastava, G. P.; Mohan, S.; Jain, Y. S. *J. Raman Spectrosc*. **1982**, *13*, 25.
(32) Edsall, J. T. *J. Chem. Phys*. **1966**, *5*, 508.
(33) Dignam, M. J.; Moskovits, M.; Robie, R. W. *Trans. Faraday Soc.* **1971**, *67*, 3306.
(34) Pearce, H. A.; Sheppard, N. *Surf. Sci.* **1976**, *59*, 205.

Table 1. Vibrational Assignments of the Bitartrate Phase Created by Adsorption of (*R*,*R*)-Tartaric Acid on Ni(110) at Room Temperature[a]

tartaric acid powder [29]		anhydrous Rochelle salt powder [30]		RAIRS data for the adsorbed bitartrate phase on metals		
				Cu(110) [2]	Ni(110) [this work]	
cm^{-1}	assignment	cm^{-1}	assignment	cm^{-1}	cm^{-1}	assignment
1741 br,vs	$\nu_{C=O}$					
		1594 br,s	ν_{OCO}^{asym}			
1453 br,s	ν_{C-O}^{acid}					
		1433 s	ν_{OCO}^{asym}	1430 sh,s	1434 sh,m	ν_{OCO}^{sym}
		1411 s	ν_{OCO}^{asym}	1410 sh,s	1401 br,m	ν_{OCO}^{sym}
1375 s	δ_{OH}^{alc}	1380 s	δ_{OH}^{alc}	1375 so	1370 sh,m	δ_{OH}^{alc}
	δ_{OH}^{alc}	1344 w	δ_{OH}^{alc}		1325 br,s	δ_{OH}^{alc}
1318 w	δ_{OH}^{acid}	1312 w		1338 s		
1255 m	+	1245 vw	δ_{C-H}	1200 w	1272 sh,w	δ_{C-H}
1220 m	δ_{C-H}	1211 vw				
1190 m		1113 w				
1134 m	ν_{C-O}^{alc}	1069 w	ν_{C-O}^{alc}	1113 s	1110 sh,s	ν_{C-O}^{alc}
1087 m						
992 w	ν_{C-C}	994 w	ν_{C-C}		999 sh,m	ν_{C-C}

[a] Literature values for solid tartaric acid powder [29], anhydrous Rochelle salt [30], and for bitartrate/Cu(110) system [2] are listed for comparison. The abbreviations s, m, w, v, sh, br, and so indicate strong, medium, weak, very, sharp, broad, and shoulder, respectively.

comparison of this spectrum with the IR spectra of Rochelle salt[30] and dipotassium tartrate,[31] where the tartaric acid is present as bitartrate ions, reveals strong similarities. In addition, this RAIR spectrum is similar to that observed from the bitartrate phase formed by (*R*,*R*)-tartaric acid on Cu(110).[2] On the basis of this, it can be surmised that adsorption on Ni(110) at room temperature leads to the formation of the bitartrate species at low coverage. This conclusion is consistent with the complete absence of the $\nu_{C=O}$ band in the 1700 cm^{-1} region of the IR spectrum and the presence of doublet ν_{OCO}^{sym} vibrations at 1434 and 1401 cm^{-1}, which is a trademark for the bitartrate system.[30,31] A complete assignment of all the vibrational bands is provided in Table 1. The appearance of only the symmetric component of the OCO stretch, ν_{OCO}^{sym}, and the absence of the asymmetric ν_{OCO}^{asym} vibration suggest that both oxygen atoms in each carboxylate group are approximately equidistant from the surface, thus rendering the ν_{OCO}^{asym} vibration inactive as a result of the RAIRS dipole selection rule. However, it should be noted that ν_{OCO}^{sym} is also strongly attenuated with a peak intensity of only 0.04%, which is substantially lower than observed, for example, for the formate/Ni(110) system[35] where the OCO plane is held perpendicular to the metal surface. From this observation, it can be concluded that the OCO planes for both carboxylate groups are largely inclined toward the surface plane. This behavior is similar to that observed for alanine[3] and glycine[36−39] on Cu(110) where the molecules straddle across the close-packed rows of the surface to achieve two-point bonding via the carboxylate and the amine functionalities, thus forcing the OCO plane toward the surface.

4.2. Nature of the Adsorption Site. The nature of the adsorption site occupied by the bitartrate species could not be directly determined from our experimental data, so we utilized DFT methods to calculate the minimum energy position. The preferred adsorption site of the molecule was initially analyzed by laterally shifting the molecular position above the Ni(110) surface. This procedure yielded an energy minimum when the center of the molecule coincided with the hollow site of the Ni surface, Figure 3. Subsequently, the molecule was relaxed in the following three different orientations above this adsorption site: (i) oriented along the [1$\bar{1}$0] direction, its center above the hollow site between Ni surface atoms, (ii) oriented along the [001] direction with the same lateral position, and (iii) oriented at an angle of 45° with respect to the close-packed crystallographic directions. However, these configurations constrain the resulting ground state severely, as they do not allow for any change of the lateral distances between the Ni surface atoms. Therefore, we sought to gain a better understanding of the final adsorption state by commencing with a fully relaxed bitartrate-Ni_4 complex and by determining the final state from there. In all cases, the adsorption energy was calculated for the bitartrate species on the clean surface. We note that this does not correspond to the overall adsorption energy of the actual surface reaction, which involves a double deprotonation of the (*R*,*R*)-tartaric acid molecule and the chemisorption of the H atoms at the surface. However, since these two processes contribute identically for all the adsorption cases considered above, the differences in computed energies correspond directly to the differences in energy of the various chemisorption events.

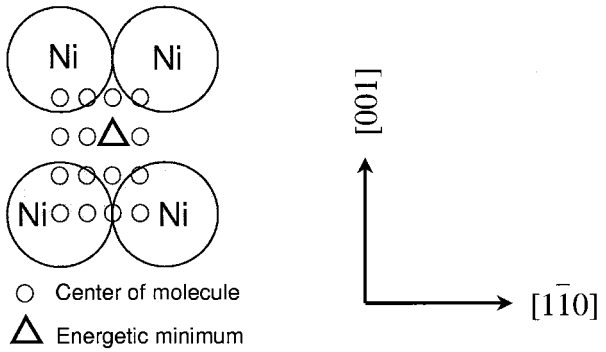

Figure 3. Grid used to determine the lateral position of the bitartrate species on the Ni(110) surface.

(35) Haq, S.; Love, J. G.; Saunders, H. E.; King, D. A. *Surf. Sci.* **1995**, *325*, 230.
(36) Booth, N. A.; Woodruff, D. P.; Schaff, O.; Giessel, T.; Lindsay, R.; Baumgärtel, P.; Bradshaw, A. *Surf. Sci.* **1998**, *397*, 258.
(37) Hasselström, J.; Karis, O.; Weinelt, M.; Wassdahl, N.; Nilsson, A.; Samant, M. G.; Stöhr, J. *Surf. Sci.* **1998**, *407*, 221.
(38) Barlow, S.; Kitching, K.; Haq, S.; Richardson, N. V. *Surf. Sci.* **1998**, *401*, 322.
(39) Nyberg, M.; Hasselström, J.; Karis, O.; Wassdahl, N.; Weinelt, M.; Nilsson, A.; Pettersson, L. G. M. *J. Chem. Phys.* **2000**, *112*, 5420.

Table 2. Optimized Bond Lengths and Angles Computed for the Various Bitartrate Structures

	bitartrate in a vacuum	bitartrate-Ni_4 in a vacuum	bitartrate adsorbed on Ni(110) aligned along [1$\bar{1}$0] geometry (i)	bitartrate adsorbed on Ni(110) aligned along [001] geometry (ii)	bitartrate-Ni_4 adsorbed on Ni(110) geometry (iv)
$Ni-O_1$		1.93	1.93	1.97	2.04
$Ni-O_2$		1.91	1.91	1.91	1.94
$Ni-O_3$		1.90	1.91	1.89	1.94
$Ni-O_4$		1.93	1.93	1.96	2.04
C_1-O_1	1.23	1.28	1.28	1.28	1.29
C_1-O_2	1.24	1.28	1.27	1.28	1.28
C_4-O_3	1.24	1.28	1.27	1.27	1.28
C_4-O_4	1.23	1.28	1.28	1.28	1.29
C_1-C_2	1.63	1.52	1.53	1.53	1.55
C_2-C_3	1.79	1.57	1.61	1.60	1.57
C_3-C_4	1.63	1.52	1.53	1.51	1.55
θ $C_1-C_2-C_3$	110	113	109	113	124
θ $C_2-C_3-C_4$	110	113	113	111	124
θ $O_1-C_1-O_2$	141	125	128	125	124
θ $O_3-C_4-O_4$	141	125	128	125	124
average angle of OCO wrt Ni surface plane		61	76	73	38.5

[a] Bond lengths are in Å, bond angles are in deg, and atoms' positions refer to Figure 5b.

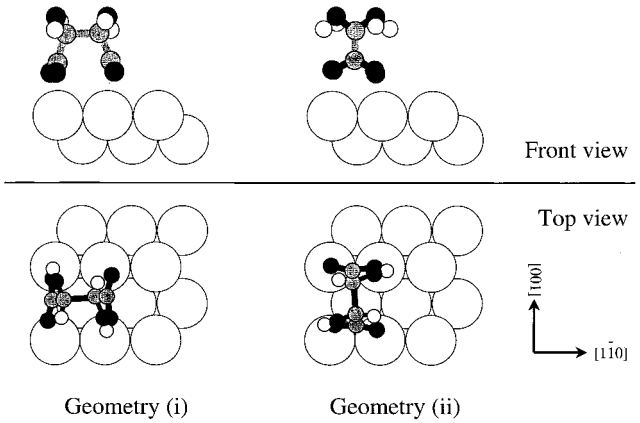

Figure 4. Adsorption configurations for the bitartrate species adsorbed on Ni(110) in geometry (i) aligned along the [1-10] axis and geometry (ii) aligned along the [001] axis.

Of the first three configurations, only (i) and (ii) lead to stable final states of bitartrate on the surface, while (iii) is significantly more unstable. In the two stable final states, Figure 4, two-point bonding of the bitartrate occurs with the oxygen atoms of both carboxylate functionalities adsorbing on top of adjacent Ni atoms, their positions in a plane parallel to the surface. This adsorption site is similar to those found for the formate species on Ni(110)[40−42] and the formate,[43,44] acetate,[44,45] and glycinate[36−39] species on Cu(110), all of which bond to the metal via the carboxylate functionality. The length of the Ni−O bonds is about 1.92 Å which is similar to the value of 1.97 Å calculated for the Cu−O bond in the bitartrate species on Cu(110)[46] and experimentally measured at 1.98 Å for formate on Cu(110).[43] Table 2 lists the bond lengths and angles for the various adsorbate configurations. Of the two geometries (i) and (ii), the adsorption energy with the molecule aligned along the [001] direction is higher by 19 kJ mol^{-1}. This is largely due to the minimization of repulsive interactions between the molecular OH groups and the Ni surface atoms. Another major consequence of these OH−Ni interactions is that the relaxation of the system with the bitartrate species attached to four adjacent nickel atoms of the surface is heavily strained. Since this inherent strain arises from the surface Ni atoms being constrained to lie close to their clean, bulk-truncation positions, we also investigated the adsorption energetics starting with a fully relaxed bitartrate-Ni_4 complex, which would be free to optimize the positions of the Ni atoms comprising the adsorption site. Interestingly, this procedure yielded an entirely different adsorption geometry, as described below.

The adsorption was mimicked in the calculation in two steps: first we attached four Ni atoms to the bitartrate molecule in its initial configuration, Figure 5a and b. Here, the interaction between the chiral OH groups of the molecule and the Ni atoms leads to twisted C−C bond angles. For the gas-phase bitartrate, all C−C bonds are in line with all carbon atoms in one plane. However, upon attachment of Ni atoms, an acute distortion in the molecule is induced whereby the C(2)−C(3) bond is skewed by about 20° with respect to each of the other C−C bonds, Figure 5b. Second, when this complex attaches itself to the Ni-(110) surface, the same interaction between the chiral OH groups of the complex and the Ni surface atoms increases this angle to 45°. The most interesting outcome of this is the pairs of Ni atoms constituting the adsorption site are now placed a significant distance apart and describe an oblique unit mesh at the surface for which all mirror planes are lost locally, Figure 5c. It would, therefore, seem that the adsorbed bitartrate conveys its chirality not just simply by its presence at the surface, but more profoundly via the footprint it places onto the surface. The Ni−O bonds in this geometry are 2.04 Å long for bonds adjacent to OH groups of the molecule and 1.94 Å otherwise, Table 2. We note that, in contrast to Cu atoms, with their closed shell of 3d electrons, electron charge in Ni atoms is easier to

(40) Jones, T. S.; Richardson, N. V.; Joshi, A. W. *Surf. Sci.* **1988**, *207*, 1948.
(41) Jones, T. S.; Ashton, M. R.; Richardson, N. V. *J. Chem. Phys.* **1989**, *90*, 7564.
(42) Ushio, J.; Papai, I.; St-Amant, A.; Salahub, D. R. *Surf. Sci. Lett.* **1992**, *262*, L134.
(43) Woodruff, D. P.; McConville, C. F.; Kilcoyne, A. L. D.; Lindner, Th.; Somers, J.; Surman, M.; Paolucci, G.; Bradshaw, A. M. *Surf. Sci.* **1988**, *201*, 228.
(44) Karis, O.; Hasselström, J.; Wassdahl, N.; Weinelt, M.; Nilsson, A.; Nyberg, M.; Pettersson, L. G. M.; Stöhr, J.; Samant, M. G. *J. Chem. Phys.* **2000**, *112*, 8146.
(45) Weiss, K.-U.; Dippel, R.; Schindler, K.-M.; Gardner, P.; Freitzche, V.; Bradshaw, A. M. *Phys. Rev. Lett.* **1992**, *69*, 3196.
(46) Barbosa, L. A. M. M.; Sautet, P. *J. Am. Chem. Soc.* **2001**, *123*, 6639.

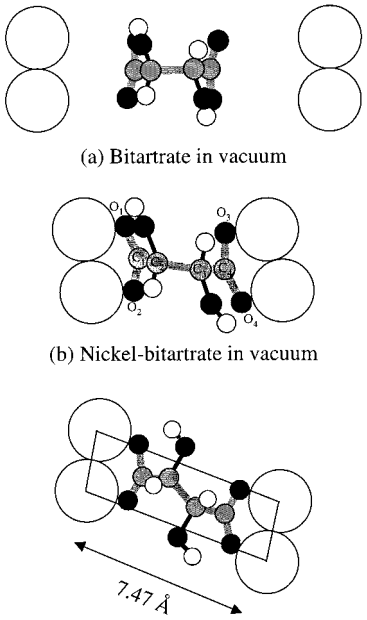

Figure 5. Progressive distortions calculated for the $C_1-C_2-C_3-C_4$ skeleton from (a) the bitartrate species in a vacuum, (b) a bitartrate-Ni_4 species in a vacuum, and (c) a bitartrate-Ni_4 species adsorbed on a Ni(110) surface. Note that in (c) the significant skewing of the molecular skeleton causes the four bonding Ni atoms to describe an oblique, chiral footprint.

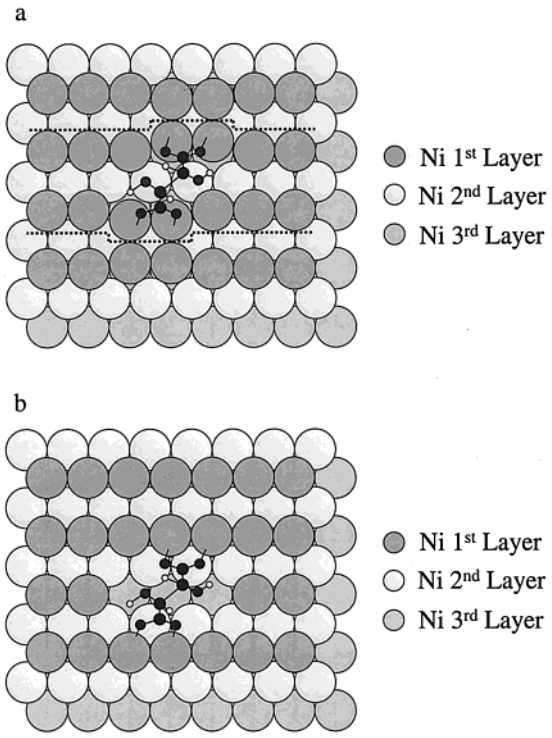

Figure 6. Schematic models to demonstrate how the relaxed bitartrate-Ni_4 footprint could be accommodated at the Ni(110) surface by local reconstruction of the surface to (a) a paired-row structure and (b) a missing-row structure.

polarize. Therefore, interactions with highly polar molecular groups, such as OH, should result in higher energy variations of different adsorption sites. In our simulations, this feature, which drives the chiral surface reconstruction, leads to a maximum of adsorption energy in configurations where the distance between the OH group and Ni surface atoms is maximized. From this we conclude that the polarization interaction is, in fact, repulsive.

The adsorption energy of an isolated bitartrate-Ni_4 complex adsorbed in this geometry on Ni(110) is 19 kJ mol^{-1} lower than that in site (i) and 39 kJ mol^{-1} lower than that in site (ii). However, if we correct for the lower coordination of the Ni surface atoms in this bitartrate-Ni complex, we find an energy advantage of 39 kJ mol^{-1} over site (i) and 19 kJ mol^{-1} over site (ii). This implies that this type of adsorption geometry will only be preferred if the Ni atoms involved in bonding to the bitartrate can relax at the surface without a change of coordination. There are two consequences of this. First, local corrosion of the nickel surface to create individually adsorbed bitartrate-Ni_4 complexes is not expected at room temperature. Second, since the Ni footprint of the adsorbed complex requires the long bridge distance between the pairs of Ni atoms to be about 7.47 Å, Figure 5c, it would not be possible to accommodate this geometry on a bulk-truncated Ni(110) surface without lateral relaxations of Ni atoms. On the basis of this, we would anticipate at least local reconstruction on the metal surface to accompany the adsorption process.

Detailed analyses of our STM images, Figure 1, support these general conclusions. The molecular structures in the STM images occupy, on average, a space of 6.8 × 4.6 $Å^2$, in good agreement with the calculated area of 7.04 × 4.98 $Å^2$ encompassing the relaxed bitartrate-Ni complex, Figure 5c. In addition, the small-scale structure of the molecular adsorption reveals severe distortions in the immediate vicinity, Figure 1a and b, extending, on average, over a 15.5 × 12.5 $Å^2$ area for a single molecule, which for the bulk-truncation surface represents an approximate 6 × 3.5 surface cell. We attribute these distortions to local restructuring of the Ni atoms to relieve molecule-induced strain at the surface created by the large adsorption footprint, with the resulting perturbation being propagated a number of atomic distances away from the adsorption center. There are two principal surface reconstructions[27,28,47−50] that are associated with the Ni(110): the paired-row and the missing-row reconstructions. Both would allow the relaxed footprint to be accommodated without loss of Ni coordination. Schematic models depicting such local reconstructions are displayed in Figure 6. In each case, the perturbation caused by the adsorbed bitartrate extends over at least a 5 × 3 unit cell. For both geometries, the OCO planes of carboxylate units are significantly inclined toward the surface plane, consistent with the RAIRS data and the calculated value of 38.5° for the adsorbed bitartrate-Ni_4 complex, Table 2. Our experimental data does not allow us to discriminate between these two reconstruction models, and a full surface structural study would be required to verify the detailed nature of this surface perturbation.

Finally, we note that the driving force for this reconstruction is sufficient for it to be manifest even for the single molecule adsorption event, that is, a critical local coverage is not required before the reconstruction is triggered. This is also supported

(47) Somorjai, G. A.; Van Hove, M. A. *Prog. Surf. Sci.* **1989**, *30*, 201.
(48) Hu, P.; Morales de la Garza, L.; Raval, R.; King, D. A. *Surf. Sci.* **1991**, *249*, 1.
(49) Raval, R.; Haq, S.; Harrison, M. A.; Blyholder, G.; King, D. A. *Chem. Phys. Lett.* **1990**, *167*, 391.
(50) Grigo, A.; Badt, D.; Wengelnik, H.; Neddermeyer, H. *Surf. Sci.* **1995**, *331−333*, 1077.

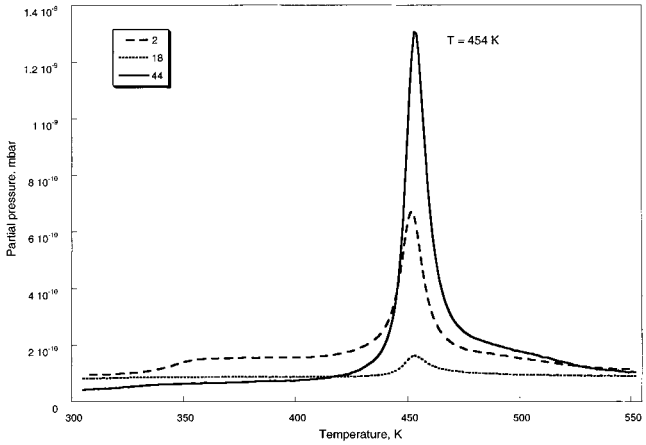

Figure 7. Thermal-programmed desorption trace obtained following adsorption of (*R*,*R*)-tartaric acid on Ni(110), showing a complete decomposition of the molecule peaking at 454 K. The broad desorption band at amu = 2 for $T = 350$ K is attributed to the recombinative desorption of coadsorbed H atoms from the surface, created during the deprotonation of the (*R*,*R*)-tartaric acid molecule upon adsorption.

by the calculations which show that the adsorbed bitartrate-Ni_4 species possesses a very large binding energy of 656 kJ mol^{-1} at a Ni(110) surface. This value is consistent with DFT calculations of individual carboxylate groups bonding to the surface, reported to be 357 kJ mol^{-1} for formate on a Cu_{10}-(110) cluster and 318 kJ mol^{-1} for acetate on a Cu_{10}(110) cluster.[44] The strength of the bitartrate−surface bond is also reflected in temperature-programmed desorption experiments, Figure 7, where an explosive decomposition releasing the products H_2, H_2O, and CO_2 is observed at 454 K, indicating that the bitartrate−metal interaction is so strong that intramolecular bonds break prior to metal−molecule bonds.

4.3. Chiral Metal Surfaces. At present, two separate approaches have been utilized to create extended chiral metal surfaces. One, demonstrated by the (*R*,*R*)-tartaric acid/Cu(110) system,[1,2,4,5] involves the assembly of chiral molecules into organized chiral arrays at the surface. In such cases, the adlayer template possesses chiral growth directions, which serve to destroy the mirror planes of the surface, and chirality is bestowed without necessarily having to introduce chiral rearrangements of the metal surface atoms. The second approach has been to utilize metal single crystals, cut to expose specific surface planes which are intrinsically chiral exposing nonstraight step edges with kink sites in which the metal atoms are arranged in a chiral configuration.[51−53] The work reported here shows that these two attributes can be fused together, with the adsorption of the chiral molecule causing an attendant chiral restructuring of the underlying metal atoms.

Perhaps the most important aspect to appreciate is that to progress from a local chiral structure to a truly extended chiral surface requires the creation of mirror chiral motifs to be severely curtailed. This is a stringent requirement, and a number of systems which exhibit local chirality, created at surfaces by adsorption of molecules[17,18] or by restructuring of the metal,[16] are unable to advance to a truly extended chiral surface because the mirror adsorption or the mirror reconstruction are equally

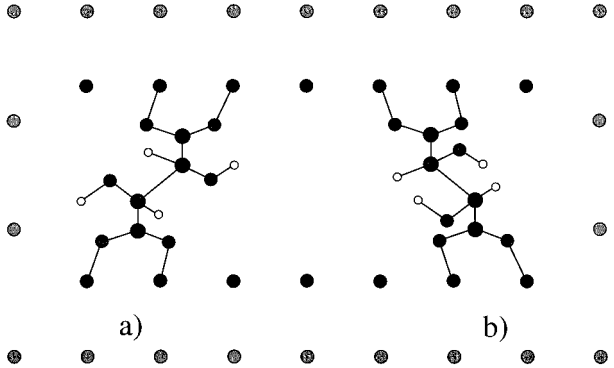

Figure 8. Depiction of the relaxed bitartrate-Ni_4 species adsorbed in twin mirror chiral footprints at the Ni(110) surface.

allowed, leading to an overall racemic system. Therefore, for our system, we sought to establish whether (*R*,*R*)-tartaric acid could also create a mirror footprint at the surface. The adsorption energies for the relaxed bitartrate-Ni_4 complex in the twin chiral footprint geometries showed in Figure 8 were computed. Our spin-polarized calculations showed that the adsorption of (*R*,*R*)-tartaric acid in the mirror footprint geometry, Figure 8b, was less favored energetically by about 6 kJ mol^{-1}. Although this is a small energy difference, a simple consideration of the Boltzmann distribution law shows that, at 300 K, this difference is sufficient to ensure that over 90% of the adsorbed bitartrate molecules adopt the preferred chiral footprint, Figure 8a, creating a highly chiral surface. For comparison, we note that in homogeneous catalysis, enantioselectivity is successfully achieved in systems operating with energy differences of ≤10 kJ mol^{-1} between two reaction pathways leading to opposite enantiomers.[54] We also note that it has recently been shown experimentally that the adsorption energies of D- and L-glucose on the intrinsically chiral Pt(643) surfaces differ by as little as 1.2 kJ mol^{-1},[55] while those of (*R*)-3-methylcyclohexanone on Cu-(643)^R and Cu(643)^S differ only by 0.9 kJ mol^{-1}.[56] Finally, chiral separations have been successfully demonstrated in systems exhibiting small binding energy differences on the order of 0.8−2.6 kJ mol^{-1}.[57]

5. Conclusions

A combination of experimental and theoretical methods has provided a detailed insight into the mode of chiral induction by adsorption of the modifier, (*R*,*R*)-tartaric acid, on the defined Ni(110) surface. Adsorption at low coverages and room temperatures leads to the creation of a very strongly adsorbed bitartrate species, which enjoys a two-point bonding to the surface via both carboxylate groups. The molecule is preferentially located above the 4-fold hollow site with each carboxylate functionality adsorbed at the short bridge site via O atoms placed above adjacent Ni atoms. Importantly, the most stable adsorption structure was achieved by a chiral relaxation of atoms in the bulk-truncation Ni(110) surface so that a large footprint with a long distance of 7.47 Å between pairs of Ni

(51) Attard, G. A. *J. Phys. Chem. B* **2001**, *105*, 3158.
(52) Sholl, D. S.; Asthagiri, A.; Power, T. D. *J. Phys. Chem. B* **2001**, *105*, 21, 4771.
(53) McFadden, C. F.; Cremer, P. S.; Gellman, A. J. *Langmuir* **1996**, *12*, 2483.
(54) Halpern, J. *Science* **1982**, *217*, 401.
(55) Attard, G. A.; Ahmadi, A.; Feliu, J.; Rodes, A.; Herrero, E.; Blais, S.; Jerkiewicz, G. *J. Phys. Chem. B* **1999**, *103*, 1381.
(56) Gellman, A. J.; Horvath, J. D.; Buelow, M. T. *J. Mol. Catal.* **2001**, *167*, 3.
(57) Lipkowitz, K. B.; Coner, R.; Peterson, M. A.; Morreale, A.; Shackleford, J. *J. Org. Chem.* **1998**, *63*, 732.

atoms could be accommodated at the surface. Thus, all the local mirror planes associated with the clean surface are destroyed locally by the adsorbed complex. Calculations show only one chiral footprint to be favored by the (*R*,*R*)-tartaric acid, with the mirror adsorption site being unstable by 6 kJ mol^{-1}. This means that, at room temperature, the same local chiral motif is expected to be repeated over 90% of the metal surface, leading to an overall chiral and very enantiospecific system.

Acknowledgment. We are grateful to the EPSRC for equipment grants, a studentship to V.H., and for providing access to the UK CSAR computing facilities under Project No. CS3013. W.H. was supported by the British Council and the National Research Council of Canada under Cooperative Research Project 98RP14.

JA012021E